A Monte-Carlo Implementation of a Geodesic Integrator for Relativistic Radiative Transfer in Accreting Black Hole Systems

Eli Golub
University of Virginia
ejg2vf@virginia.edu

May 11, 2018

Abstract

We describe the implementation of a relativistic geodesic integrator into a Monte-Carlo radiative transfer code intended for computing the spectra produced from thermal emission in optically thick accretion disks around a black hole. We first implemented the integrator and tested it by computing geodesics in the Schwarzschild metric and demonstrated agreement with geodesics computed by the relativistic radiative transfer code *geokerr* (Dexter & Agol 2009). We then implemented the integrator as a module to transport photons in the existing Monte-Carlo radiation transfer code *mcgrid* (Davis et al. 2009). We tested our newly implemented transport module by computing transfer through a cylindrical grid geometry. Next, we demonstrated that it could produce a black-body spectrum. Finally, we tested the code by transporting photons through a transparent grid and compared the exit positions of the particles for different step sizes.

1 Introduction

A black hole is a compact region of spacetime that possesses such a large gravitational potential that not even light can escape. In general, there are two types of black holes: stellar-mass black holes (SBHs) and supermassive black-holes (SMBHs). SBHs are typically less than 100 solar masses and form when the core of a core-collapse supernova is sufficiently massive enough to overcome neutron degeneracy pressure. The mechanism for SMBH formation is still widely debated, but SMBHs - whose mass ranges from millions to several billion solar masses - are thought to have formed from a merger of multiple SBHs [1] (Schutz 2009).

[1] Other theories of SMBH formation range from the collapse of massive gas clouds in the early stages of galaxy to a gradual accretion of enormous amounts of material over millions of years (Schutz 2009).

However, regardless of their mass, black holes are described by the fact that one can fall into them, but never exit. Thus, there must be a point of no-return near the black hole in which a boundary exists. This is the black hole's most prominent feature and is known as the event horizon: a hypersurface separating spacetime points that are connected at infinity by a time-like path from those that are not.

Here, infinity is taken as a proxy for points considerably far from the event horizon. We can then imagine that spacetime sufficiently positioned from the singularity is best approximated by an asymptotically flat, Minkowski space.

While light cannot escape once inside the event horizon, black holes still remain astrophysically interesting because infalling material just beyond the event horizon produces emission through accretion flows. The emission from this accretion is what allows us to observe accreting black hole systems.

Accreting black holes occur in binary systems, such as a star near a black hole. If the star expands in close binary, material from the star can accrete onto the black hole. The infalling material of the star forms an accretion disk around the black hole.

The most well described accretion flow state onto a black hole is that of a geometrically thin, optically thick disk (Shakura & Sunyaev 1973). The accretion process is a complex and difficult problem to understand and so considerable effort has been devoted to creating theoretical models of accretion flows.

One important accreting system is a black hole X-ray binary (BHB), where material from a companion star accretes onto a black hole, producing X-ray emission. It is widely believed that a fraction of this X-ray emission is a result of thermal emission from an optically thick accretion disk (Shakura & Sunyaev 1973). Spectral modeling of these sources therefore provides both a means for testing accretion disk theory in the strong gravity around a black hole and deducing properties of the black hole itself, such as the mass of the central black hole, the accretion rate, and the orientation of the disk itself (Davis et al. 2009).

In order to model the spectra from accretion disks, we need a means to simulate relativistic radiative transfer. A considerable amount of effort as been devoted to theoretically developing spectral models of such disks for comparison with observations (e.g. Kolykhalov & Sunyaev, 1984; Shimura & Takahara, 1995; Sincell & Krolik, 1998; Hubeny et al. 2001; Davis & Hubeny, 2006; Davis et al. 2009).

Most of these previous efforts rely on the simple model of Shakura & Sunyaev (1973). More recent models involve expensive numerical simulations of relativistic radiative transfer calculations. The goal of these simulations is to produce simulated spectra and compare them to observed spectra. Specifically, observational motivations for radiative transfer codes include, but are not limited to, accreting black hole systems, BHBs, and active galactic nuclei (AGN).

In this paper, we summarize our implementation of a geodesics integrator in a Monte-Carlo transfer code. We describe our implementation and tests of the integrator in Section 2. In section 3, we summarize the methods of the Monte-Carlo radiative transfer method and the addition of our integrator as a module to the existing code *mcgrid*. Finally, we describe the tests of the module in Section 4.

2 Geodesic Integration

As one approaches a black hole's event horizon, spacetime becomes more and more warped, theoretically approaching infinite curvature at the singularity. It is therefore important to model relativistic effects for photons in a curved spacetime. In flat Euclidean space, one typically uses Cartesian coordinate systems since they have straight world lines orthogonal to each other. This is the simplest coordinate system since the coordinate basis vectors are constant, and all the field vectors are unit vectors with the same direction.

There are also flat spacetime coordinate systems in which the world lines of particles are curved. In such metrics, these lines are known as geodesics: a curve whose tangent vectors remain parallel if they are transported along it (Schutz 2009). These coordinate systems are known as curvilinear coordinate systems.

In general relativity, the simplest black hole is spherically symmetric with zero spin. In this regime, Einstein's equations are solved using the Schwarzschild metric given by equation (4), where the radius of the event horizon is known as the Schwarzschild radius, given by equation (5). Birkhoff's theorem establishes that the Schwarzschild solution (equation 4) is the only spherically symmetric, asymptotically flat solution to Einstein's vacuum field equation, so we can assume that the line element describing spacetime outside a non-spinning black hole is given by Schwarzschild metric (Misner et al. 1973).

Schwarzschild coordinates, however, are limited in the sense that they can only describe non-spinning black holes. SBHs are thought to retain the rotation (or at least some fraction of) the original star. These black holes have non-zero spin and are known as Kerr black holes, since the are described by the Kerr metric in equation (10). The Kerr black hole is axially symmetric but not spherically symmetrical (i.e. only rotationally symmetric about the angular-momentum axis). Kerr black holes are described using Boyer-Lindquist coordinates (t, r, θ, ϕ), where ϕ is the angle around the axis of symmetry, t is the time coordinate in which everything is stationary, and r and θ are similar to those spherically symmetric r and θ in the Schwarzschild metric. However, the Kerr radial coordinate, r, cannot be defined as an area coordinate since there are no metric two-spheres in Kerr spacetime.

In conventional radiative transfer, photon trajectories are best defined in Minkowski spacetime: a flat, non-Euclidean space. In this metric, geodesics are trivial in the sense that they travel along straight world lines of zero proper length.

General relativistic radiative transfer differs from conventional radiative transfer because the world lines of two nearby particles do not generally remain parallel. Thereby, photon trajectories in these Riemannian [2] spaces are no longer trivial. While Riemannian spaces still remain locally flat, the locally straight lines that the photons follow become geodesics, as they are now confined to a curved spacetime.

The governing equation for general relativistic photon transport is defined by the geodesic

[2] A Riemannian space is characterized by a metric that gives positive-definite magnitudes of vectors. Moreover, this is a space where points viewed in a small, localized domain are approximately Euclidean, but become more non-Euclidean from a global perspective (Schutz 2009).

equation (Carroll 2004):

$$\frac{dk^{\alpha}}{d\lambda} = -\Gamma^{\alpha}_{\mu\nu} k^{\mu} k^{\nu} \tag{1}$$

where k^{α} is the wave four-vector and is defined as

$$k^{\alpha} = \frac{dx^{\alpha}}{d\lambda} \tag{2}$$

This equation defines the affine parameter, λ. The connection coefficients in equation (1) are then defined as

$$\Gamma^{\alpha}_{\mu\nu} = \frac{1}{2} g^{\alpha\gamma} (g_{\gamma\mu,\nu} + g_{\gamma\nu,\mu} - g_{\mu\nu,\gamma}) \tag{3}$$

These coefficients can be defined in any coordinate basis and thus in several different metrics. The photon paths are obtained by integrating equations (1) and (2) in a general metric. This includes curvilinear coordinates in a flat spacetime or the curved spacetime of a black hole. For example, the Schwarzschild metric is given by

$$\begin{aligned} ds^2 &= -\left(1 - \frac{r_S}{r}\right)^2 dt^2 + \left(1 - \frac{r_S}{r}\right)^{-1} dr^2 \\ &\quad + r^2 \left(d\theta^2 + sin\theta^2 d\phi^2\right) \end{aligned} \tag{4}$$

where r_S is the Schwarzschild radius, given by

$$r_S = 2M \tag{5}$$

and equations (4) and (5) are written in geometrized units (i.e. $c = G = 1$).

The majority of the computational expense of the radiative transfer algorithm are expected to be due to integrating the geodesic equation - particularly, evaluating the connection coefficients in equation (3). In order to minimize computational expenditures, we chose an algorithm that would most optimally minimize the number of evaluations of the connection coefficients. Following Dolence et al. (2009), we utilized a Verlet velocity algorithm. For geodesics, the solution of the geodesic equation becomes

$$x^{\alpha}_{n+1} = x^{\alpha}_{n} + k^{\alpha}_{n} \Delta\lambda + \frac{1}{2} \left(\frac{dk^{\alpha}}{d\lambda}\right)_{n} (\Delta\lambda)^2 \tag{6}$$

$$k^{\alpha}_{n+1,p} = k^{\alpha}_{n} + \left(\frac{dk^{\alpha}}{d\lambda}\right)_{n} \Delta\lambda \tag{7}$$

$$\left(\frac{dk^{\alpha}}{d\lambda}\right)_{n+1} = -\Gamma^{\alpha}_{\mu\nu} \left(X_{n+1}\right) k^{\mu}_{n+1,p} k^{\nu}_{n+1,p} \tag{8}$$

$$k^{\alpha}_{n+1} = k^{\alpha}_{n} + \frac{1}{2} \left(\left(\frac{dk^{\alpha}}{d\lambda}\right)_{n} + \left(\frac{dk^{\alpha}}{d\lambda}\right)_{n+1} \right) \Delta\lambda \tag{9}$$

The Verlet algorithm was chosen because it only evaluates the connection coefficients once per step. Specifically, the algorithm obeys the following basic sequence. The first result is obtained from equation (9), after which we used $k^{\mu}_{n+1,p} = k^{\mu}_{n+1}$ to recompute equation (8) and then again calculate the wave-vector in equation (9). This sequence is repeated until the variance in the wave-vector ($\Delta\lambda$) between successive estimates is below a certain threshold. This threshold was taken to be 10^{-3}. These iterations do not require any additional evaluations of $\Gamma^{\alpha}_{\mu\nu}$, thus saving excessive computational expenditures.

The accuracy of the algorithm was then tested by comparing the results to those produced by the relativistic radiative transfer FORTRAN

code *geokerr* developed and implemented by Dexter & Agol (2009). Dexter & Agol (2009) presented a method for rapidly and accurately calculating null geodesics in curved spacetime. While their algorithm can be used in a wide variety of applications, *geokerr* is most applicable to relativistic radiative transfer in accreting black hole systems.

Their code computes geodesics in the Kerr metric. In Boyer-Lindquist coordinates (t, r, θ, ϕ), the Kerr line element can be written as

$$ds^2 = -\rho^2 \frac{\Delta}{\Sigma^2} dt^2 + \frac{\Sigma^2}{\rho^2} \left(d\phi - \frac{2ar}{\Sigma^2} dt \right)^2 sin^2\theta + \frac{\rho^2}{\Delta} dr^2 + \rho^2 d\theta^2,$$

where

$$\Delta = r^2 - 2r + a^2 \tag{10}$$

$$\rho^2 = r^2 + a^2 cos^2\theta \tag{11}$$

$$\Sigma^2 = \left(r^2 + a^2\right)^2 - a^2 \Delta sin^2\theta, \tag{12}$$

here, *a* is defined as the angular momentum of the black hole. Again, we are using geometrized units (i.e. $c = G = M = 1$) (Dexter & Agol, 2009).

In order to minimize computational expenditures, Dexter & Agol (2009), along with Rauch & Blandford (1994), reduced the equations of motion derived from the Hamilton-Jacobi equation to Carlson's elliptic integrals. This simplified algebraic manipulation and allowed all coordinates to be computed semi-analytically (Dexter & Agol, 2009).

We compared our integrator to *geokerr* by initializing photon trajectories with the same initial x^α and k^α. Here, x^α is the photon's initial position and k^α is its initial wave-vector. We then followed the geodesics as they propagated from their initial location to large radii. Figure 1 shows an example for integration around a non-spinning black hole in the Schwarzschild metric. This corresponds to a spin of $a = 0$ in Boyer-Lindquist coordinates.

Twenty geodesics were initialized from an initial position of four gravitational radii (i.e. $r_{int} = 4R_g$) from the black hole's event horizon, depicted in Figure 1 as a black circle. The geodesics were contained in the same plane, isotropically distributed in initial direction. For simplicity, we do not show geodesics that entered the black hole's event horizon. The solid lines in Figure 1 represent the geodesics computed by *geokerr*, whereas the dots are those computed by our integrator. The different colors are merely meant to distinguish one geodesic from another. We find clear agreement between our integrator and *geokerr*, indicating that our implementation is working correctly.

3 Monte-Carlo Transfer

The geodesic integrator was then implemented into the Monte-Carlo (MC) radiative transfer code, *mcgrid*. As described by Davis et al. (2009), *mcgrid* reads in a grid of densities and temperatures from a 3-dimensional snapshot of a simulation. Once set, these parameters are taken to be constant throughout the MC calculation. The code supports cartesian, cylindrical, and spherical metrics in flat spacetimes.

First, the electron density, free-free emissivity, and absorptivity are computed for each zone in the 3d grid. The MC code then propagates photon packets through the cylindrical grid until they either escape or are absorbed. The code assumes each grid zone is homogeneous in den-

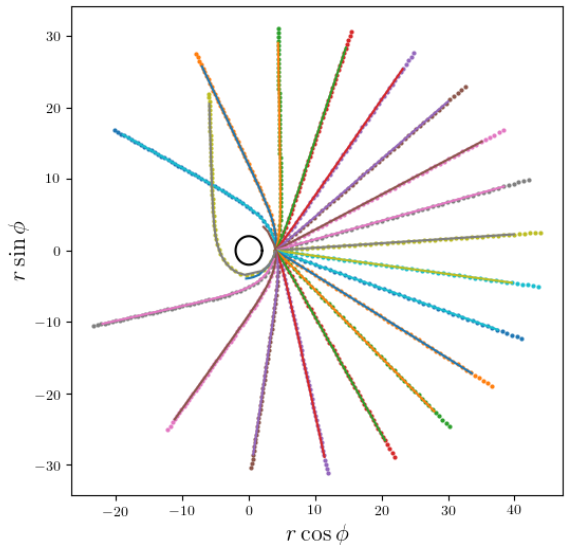

Figure 1: The above graph depicts twenty geodesics initialized at $r_{int} = 4R_g$ and transported through a transparent grid. Our integrator's geodesics are represented as dots. The geodesics computed by *geokerr* are represented as lines.

sity and temperature.

The initial location of each photon packet is randomly positioned within the grid. Each packet is then assigned a weight based upon the emissivity of its initial grid zone. The packet's initial direction vector is randomly determined from an isotropic distribution. Initially unpolarized, the photons' energy is also randomly chosen and consequently assigned a weight in order to approximate the frequency dependence of the free-free emissivity.

Once initialization is complete, the absorption and electron scattering mean free paths are computed for the appropriate energy. The photons are then propagated along a ray pointing along the direction vector by some randomly chosen optical depth determined from an exponential distribution. For the photon packet to be propagated into a neighboring grid zone, the optical depth must be sufficiently large.

Each time the packet moves into a new grid zone, the mean free paths are updated. Propagation continues until the photon either escapes or moves the prescribed optical depth. If the packet escapes, its weighted distribution is added to the output arrays corresponding to its final direction and energy. A new packet is then initialized. This process is then repeated.

If the photon remains in the cylinder, its weight is reduced by the ratio of absorption to total opacity. The total opacity is the sum of the absorption and electron scattering opacity. In the event that the packet's weight falls below a predetermined minimum weight, it is absorbed. A new packet is then initialized, and the process repeats. Otherwise, the packet is assumed to have scattered and its energy, direction vector, and polarization vector are updated.

Although the ultimate goal of our work is to use our integrator for curved spacetimes, our initial implementation focused on curvilinear coordinate systems in flat spacetimes. However, even in flat space a geodesic integrator is needed to follow geodesics when directions are specified relative to a curvilinear coordinate system.

The existing transfer method in *mcgrid* contains transport modules for cartesian, cylindrical, and spherical coordinate systems. However, it assumes that the wave vector, k^α, is defined in the cartesian basis (k_x, k_y, k_z). Therefore, one simply computes the intersection of a straight

line defined by k^α with the curved faces of the grid zone. The method then computes the rays' intersection with the nearest grid face and moves the packet to that face.

We supplemented these existing transfer methods with our geodesic integrator. The new transfer method does not assume that the wave-vector is defined in a cartesian basis. Rather, k^α follows polar coordinates (e.g. k_r, k_ϕ, k_z in cylindrical coordinates). Just as before, we compute the distance to the nearest grid face and move the photons to that boundary. Once the photons cross grid boundaries, an average of all of the opacities in the two neighboring zones is used to compute the total optical depth. The total optical depth is then reduced by a step size taken to be a fraction of the zone size. This step size is adjusted adaptively to required accuracy (Dolence et al. 2009). Limiting the step size ensures that the packet does not cross multiple boundaries at one time. The photon takes multiple steps until the requisite optical depth is obtained.

One advantage of replacing the existing transfer method with our geodesic integrator is that one can compute any curvilinear system by supplying a metric and computing the connection coefficients $\Gamma^\alpha_{\mu\nu}$ given by equation (3). By defining the wave-vector in cylindrical coordinates, for example, we can more easily model the cylindrical geometry of accretion disks.

4 Test Results and Conclusion

In this section, we test our code using a cylindrical grid. The general metric in cylindrical coordinates (r, ϕ, z) is:

$$ds^2 = \begin{bmatrix} -1 & 0 & 0 & 0 \\ 0 & 1 & 0 & 0 \\ 0 & 0 & r^2 & 0 \\ 0 & 0 & 0 & 1 \end{bmatrix} \tag{13}$$

The non-vanishing Christoffel symbols are given as:

$$\Gamma^r_{\phi\phi} = -r \tag{14}$$

$$\Gamma^\phi_{\phi r} = \Gamma^\phi_{r\phi} = -1/r \tag{15}$$

The vanishing Christoffel symbols are then:

$$\Gamma^r_{rr} = \Gamma^r_{r\phi} = \Gamma^r_{\phi r} = \Gamma^\phi_{rr} = \Gamma^\phi_{\phi\phi} = 0 \tag{16}$$

where all Christoffel symbols involving z are also zero:

$$\Gamma^\alpha_{z\beta} = \Gamma^\alpha_{\beta z} = 0 \tag{17}$$

4.1 Test 1: Black-Body Spectrum

In this section, we demonstrate that the geodesic integrator, once implemented as a module into *mcgrid*, can produce a black-body spectrum. To do so, we transported photons through the cylindrical grid seen in Figure 2. The grid is isothermal in temperature.

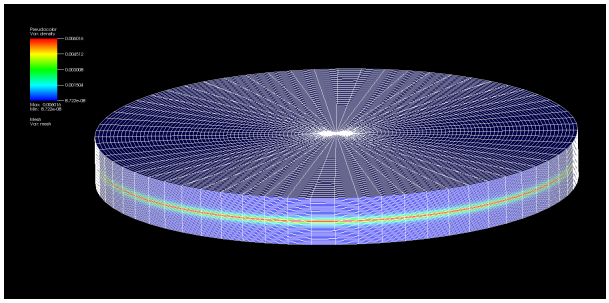

Figure 2: The above figure is a cylindrical grid of isothermal temperature through which photons were transported. The density is logarithmic and varies in the vertical direction. The grid mesh on the surface of the cylinder shows the zones through which the photons are propagated.

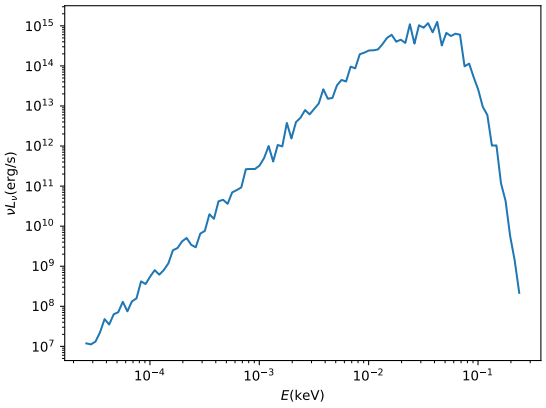

Figure 3: The above figure is the black-body spectrum produced from relativistic radiative transport through the grid in Figure (2). The vertical axis is in luminosity units and the horizontal axis is photon energy.

The density of the grid is logarithmic and varies in the vertical direction. The minimum density of the grid is $\rho_{min} = 8.722 \times 10^{-8}$ g/cm^3 and the maximum to be $\rho_{max} = 6.016 \times 10^{-3}$ g/cm^3. The grid mesh superimposed on the cylinder's surface represents the grid zones through which the photon packets are propagated. The boundary conditions are that the grid is periodic in the azimuthal direction ϕ. The photon can also freely escape from vertical boundaries and be absorbed in the radial direction.

Once the grid in Figure (2) was generated, we produced the black-body spectrum in Figure 3. Note that the y-axis is in units of erg/s rather than $erg/cm/s$ because the radiation is integrated over the surface area of the grid.

Particularly, Figure (3) was produced for 100 photons per grid zone, propagated through the grid in Figure (2) with absorption and no scattering. There were 96 energy bins, and 8 polar angle and azimuthal bins. We plotted the spectrum across four decades of photon energy in units of keV, as illustrated by the range of the x-axis. The spectrum in Figure (3) matches the black-body spectrum for a disk with an isothermal temperature of $10^5 K$.

4.2 Test 2: Final Position

Our second test was purely a test of the transfer module, so we constructed a grid like that shown in Figure (2) but set the scattering and absorption opacity to zero so that photons move from their initial position to the nearest boundary without interaction. This is a useful test of the integrator because the photon crosses many grid zones before reaching the boundary. We first picked a random initial position and grid zone. We then computed the intersection of the

photon's straight line path with the radial or vertical boundary to acquire the final radius, angle, and height (r_f, θ_f, z_f) the particle traveled in the cylindrical grid.

Namely, the straight line distance to the nearest radial or vertical boundary for each photon was calculated using the initial radius, angle, and height (r_i, θ_i, z_i):

$$\Delta_i = \sqrt{(x_f - x)^2 + (y_f - y)^2 + (z_f - z)^2} \quad (18)$$

where

$$x = r_i \cos\theta_i, x_f = r_f \cos\theta_f \quad (19)$$

$$y = r_i \sin\theta_i, y_f = r_f \sin\theta_f \quad (20)$$

$$z = z_i \quad (21)$$

Finally, we used the geodesic integrator to step through the grid until the photon exited and compared the final position with r_f, θ_f, and z_f.

During the time in which this paper is being written, the test to compute the final position of the particle is not functioning properly. Namely, the code compiles and runs these tests correctly since the final position for the particles in a straight line were computed correctly, but the integrator is not producing values entirely consistent with these results. We speculate that the issue is contained in the integrator's transfer function.

4.3 Conclusion

Once we are able to correctly test the method in cylindrical coordinates, the next step is to test the integrator in spherical-polar coordinates. The goal is to then generalize the method for a fully relativistic treatment. Once this is in place, we intend to use the code to model the spectra from relativistic accretion flows.

References

Carroll, Sean M. Spacetime and Geometry: An Introduction to General Relativity. Addison Wesley, 2004.

Davis S. W., Blaes O. M., Hirose S., Krolik J. H., 2009, ApJ, 703, 569

Davis, S. W., Hubeny, I., 2006, ApJ Suppl. 164, 530.

Dexter, J., Agol, E., 2009, ApJ, 696:1616-1629

Dolence J. C., Gammie C. F., Mocibrodzka M. and Leung P. K. 2009 ApJ Suppl., 184, 387

Hubeny, I., Blaes, O., Krolik, J. H., Agol, E. 2001, ApJ 559, 680

Kolykhalov, P. I., Sunyaev, R. A. 1984, Advances in Space Research, 3, 249

Rauch K. P., Blandford R. D., 1994, ApJ, 421, 46

Schutz, Bernard F. A First Course in General Relativity. Cambridge University Press, 2009.

Shakura, N. I., Sunyaev, R. A. 1973, A&A, 24, 337

Shimura, T., Takahara, F. 1995, ApJ, 445, 780

Sincell, M. W., Krolik, J. H. 1998, ApJ, 496, 737